

“© 2012 IEEE. Personal use of this material is permitted. Permission from IEEE must be obtained for all other uses, in any current or future media, including reprinting/republishing this material for advertising or promotional purposes, creating new collective works, for resale or redistribution to servers or lists, or reuse of any copyrighted component of this work in other works.”

Electronically Steerable 1D Fabry-Perot Leaky-Wave Antenna Employing a Tunable High Impedance Surface

Raúl Guzmán-Quirós, *Student Member, IEEE*, José Luis Gómez-Tornero, *Member, IEEE*, Andrew R. Weily, *Member, IEEE*, and Y. Jay Guo, *Senior Member, IEEE*

Abstract— A novel fixed-frequency electronically-steerable one dimensional (1D) leaky-wave antenna is presented. The antenna is based on a parallel-plate waveguide loaded with a planar partially reflective surface and a tunable high impedance surface (HIS), which creates a 1D Fabry-Perot leaky-waveguide. The tunable HIS consists of printed patches loaded with varactor diodes that allow the electronic tuning of the cavity resonance condition. Using a simple Transverse Equivalent Network, it is theoretically shown how the variation of the varactors' junction capacitance allows the scanning of the antenna pointing angle from broadside towards the endfire direction at a fixed frequency. Experimental results of an antenna prototype operating at 5.6 GHz are reported, demonstrating that the new reconfigurable leaky-wave antenna can provide electronic beam scanning in an angular range from 9° to 30°.

Index Terms— Leaky-wave antennas (LWA), reconfigurable antennas, electronic beam scanning, high impedances surfaces, partially reflective surfaces, electromagnetic band gap structures, frequency selective surfaces.

I. INTRODUCTION

SCANNING of the main beam direction is an inherent property in one-dimensional Leaky-Wave Antennas (1D LWAs), which is usually achieved by sweeping the frequency of the input microwave signal [1-3]. For many applications, however, operation at a fixed frequency is required [4]. Various technologies and topologies have been proposed in recent decades to create fixed-frequency electronically-steerable 1D LWAs [5-24]. In all cases, an active device is employed to produce the electronically controlled change in the leaky-line boundary conditions, thus altering the leaky mode (LM) complex propagation constant ($k = \beta - j\alpha$) and producing the associated change in its pointing direction (noting $\sin \theta_{RAD} \approx \beta/k_0$, where θ_{RAD} is measured from the broadside direction) [2]. For instance, p-i-n diodes have been added to dielectric rod LWAs [5,10] or microstrip LWAs [19], obtaining a discrete change in θ_{RAD} . Similar discrete changes

are reported when introducing photosensitive switches in dielectric slab LWAs [9], or electronic switches in multi-port microstrip LWAs [20],[21]. Continuous scan of the main beam has been obtained in corrugated ferrite LWAs [6],[7], microstrip LWAs over a ferroelectric substrate [17], photoinduced plasma grating LWAs [8], and microstrip LWAs loaded with photosensitive silicon substrates [14], by respectively using magnetic/electric fields or optical signals to control θ_{RAD} . However, the most used active device to electronically control 1D LWAs in the microwave range is the varactor diode, which has been applied to multitude of leaky lines as the slotline [11], the coplanar waveguide [12], the first higher-order mode microstrip line [13], the composite right-left handed microstrip line [15],[16], the microstrip log-periodic line [18], the half-mode microstrip line [22],[24], and the half-mode substrate-integrated waveguide [23].

In this paper, we present a new configuration of reconfigurable 1D LWA to achieve fixed-frequency beam steering, which is based on a 1D Fabry-Perot (FP) leaky-waveguide recently proposed in [25]. In the antenna, varactor diodes are added to the High Impedance Surface (HIS) substrate in order to achieve electronic control of the pointing angle. A simple transverse equivalent network (TEN) is used to analyze the LWA and provide a theoretical foundation for the proposed mechanism to steer the beam. An experimental prototype of the antenna operating at 5.6 GHz was designed and tested. Good agreement between theoretical predictions and experimental results are obtained.

The paper is organized as follows. The working principle of the new reconfigurable 1D LWA is described in Section II. It is shown that, using the transverse equivalent network (TEN), the dispersion of the associated LM (please spell it out as it is the first time this is used) is a function of the varactor junction capacitance. The dispersion curves prove essential for the computer-aided design of the antenna, and particularly for the optimization of the scanning range. All the TEN analysis results are validated with full-wave simulations. Section III reports experimental results obtained from a fabricated prototype operating at 5.6 GHz, showing an electronically-controlled scanning region from $\theta_{RAD} = 9.2^\circ$ to $\theta_{RAD} = 34.2^\circ$ as the varactors' biasing DC voltage is varied from 4.5V to 18.2V. Practical limitations of the proposed antenna for scanning angles close to endfire are also discussed. Finally, Section IV summarizes the main conclusions of this work.

Manuscript received November 11, 2011. This work has been supported by Spanish National project TEC2010-21520-C04-04, Spanish Regional Seneca project 08833/PI/08, and Australian project XXXX.

R. Guzmán-Quirós and J.L. Gómez-Tornero are with the Department of Communication and Information Technologies, Technical University of Cartagena, Cartagena 30202 Spain (phone: +34-968326531; fax: +34-968325973; e-mail: josel.gomez@upct.es). A. Weily and Y. Jay Guo are with the CSIRO ICT Centre, Epping, NSW 1710, Australia.

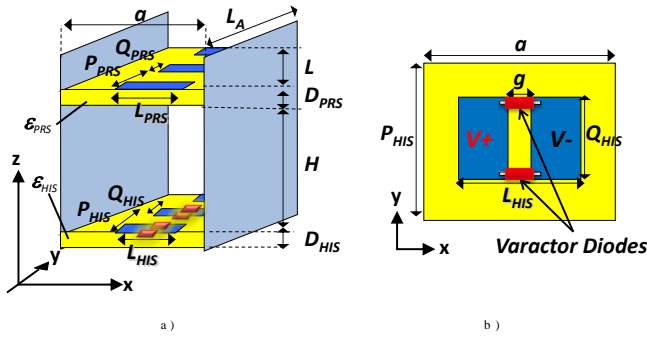


Fig. 1. a) Scheme of the proposed Reconfigurable 1D LWA b) Detail of tunable High Impedance Surface. (a=25 mm, H=25.2 mm, L=13.6 mm, D_{HIS}=1.524 mm, ε_{HIS}=3, P_{HIS}=30 mm, Q_{HIS}=14 mm, L_{HIS}=17 mm, g=1 mm, D_{PRS}=0.8 mm, ε_{PRS}=4.4, P_{PRS}=20 mm, Q_{PRS}=18 mm, L_{PRS}=22 mm)

II. RECONFIGURABLE 1D LEAKY-WAVE ANTENNA

The proposed configuration of 1D reconfigurable LWA and its main geometrical parameters are shown in Fig.1-a. The structure is inspired by the passive antenna presented in [25], where a parallel-plate waveguide (PPW) was loaded with two passive printed-circuit boards (PCBs): a top Partially Reflecting Surface (PRS) and a bottom High Impedance Surface (HIS) (see Fig.1-a). Both PCBs are formed by periodic arrays of resonant metallic patches printed on thin dielectric substrates. The two PCBs are separated at a distance H , comprising a one-dimensional Fabry-Perot (FP) resonant cavity which allows the propagation of a perturbed TE_{01} leaky mode. Since these types of antennas combine a host PPW with PCBs, they are known as hybrid waveguide printed-circuit LWAs [25],[26]. As demonstrated in [25], this 1D FP PRS-HIS LWA allows the leakage rate to be adjusted by changing the resonant length of the PRS patches (L_{PRS} in Fig.1), while the resonant length of the HIS patches (L_{HIS} in Fig.1) controls the pointing angle at a fixed design frequency. Using these previous results, a reconfigurable version of this 1D LWA is envisaged by introducing varactor diodes in the middle of the HIS resonant patches, as illustrated in Fig.1-b. Similar types of tunable HIS have been used to design reconfigurable reflectors [27],[28], reconfigurable reflectarrays [29], or tunable Frequency Selective Surfaces [30]. Also, an electronically tunable HIS was applied in [31] to transform a surface-wave into a backward or forward leaky-wave, thus achieving beam scanning from a two-dimensional textured surface. In [32],[33], a tunable HIS was applied to tune the operating frequency of low profile 2D FP LWAs, and similar reconfigurability was demonstrated in [34] for a tunable HIS fed by a bow-tie antenna. To the best of the authors' knowledge, it is the first time that a tunable HIS is applied to the design of a fixed-frequency electronically-scanned one-dimensional Fabry-Perot LWA.

In the following subsection, a simple but accurate TEN is developed to obtain the complex propagation constant of the leaky-mode which operates in the proposed reconfigurable LWA, as a function of its main parameters. These dispersion curves give physical insight into the operating principle and design rules of the proposed LWA, and lay a theoretical foundation for the steerability of the antenna main beam. Analysis of reconfigurable LWA using a TEN

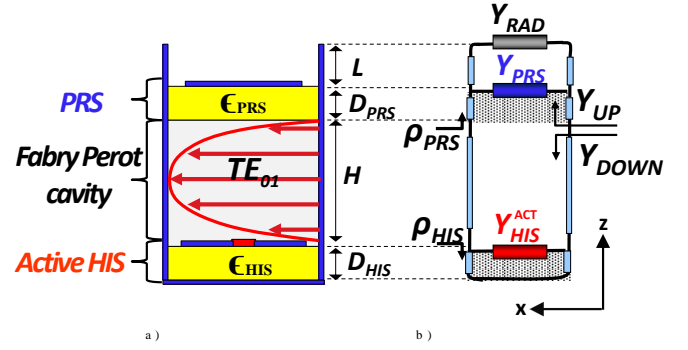


Fig. 2. a) Cross section of the reconfigurable 1D FP-PRS-tunable HIS LWA b) Transverse Equivalent Network (TEN) of the structure.

The Transverse Resonance Method (TRM) is a simple and powerful analysis tool widely used in the design of LWAs [2],[35],[36]. Particularly, as it was demonstrated in [25], the TRM allows efficient analysis and design of the passive version of the 1D FP PRS-HIS LWA. For the analysis of the reconfigurable version of this LWA, it is necessary to extend the TRM approach proposed in [25]. The key feature of the TRM is the development of an appropriate Transverse Equivalent Network (TEN) that accurately models the cross section of the antenna, which in our case is shown in Fig.2. The constituent parts of this TEN are well described in [25], with the most important parts being the equivalent admittances which model the top PRS and the bottom HIS (Y_{PRS} and Y_{HIS} in Fig.2-b). In this work, the necessary novelty required to model the tunable HIS admittance as a function of the varactors' junction capacitance C_j is introduced in the TEN formulation.

As explained in [37], the pole-zero method proposed by Maci et al. in [38] can be expanded to take into account more optimization parameters beyond frequency in the design of 1D LWA. For instance, the effect of the resonating length of the PRS patches (L_{PRS} in Fig.1-a) can be efficiently modeled by using the following analytical pole-zero expansion for Y_{PRS} [37]:

$$Y_{PRS}(k_y, L_{PRS}) = j \frac{L_{PRS} [L_{PRS} - L_{PRS_z1}(k_y)] \dots [L_{PRS} - L_{PRS_zn}(k_y)]}{[L_{PRS} - L_{PRS_p1}(k_y)] \dots [L_{PRS} - L_{PRS_pn}(k_y)]} \quad (1)$$

where the location of the poles and the zeros depend on the longitudinal wavenumber k_y , which is related to the leaky-mode incidence (or radiating) angle by $\sin \theta_{inc} = \text{real}(k_y)/k_0$.

Fig.3 illustrates the magnitude and phase of the reflection coefficient presented by the PRS (ρ_{PRS} in Fig.2-b) as a function of L_{PRS} for the design frequency of 5.6 GHz, and for three different incidence angles. As explained in [25], L_{PRS} must be properly chosen to tune the PRS reflectivity in order to control the antenna radiation efficiency. The rest of the geometrical parameters of the PRS are fixed, so patches of width $Q_{PRS}=18\text{ mm}$ separated at a distance $P_{PRS}=20\text{ mm}$, are printed on FR4 substrate ($\epsilon_{PRS}=4.4$, $D_{PRS}=0.8\text{ mm}$). As shown in Fig.3, good agreement is observed between the analytical pole-zero model of the PRS admittance (1) and full-wave results obtained with commercial Finite Element Method (FEM) solver HFSS. $L_{PRS}=22\text{ mm}$ is chosen to provide a PRS reflectivity above 0.9 for all scanning angles, as shown in Fig.3. The main novelty of the proposed TEN is in the

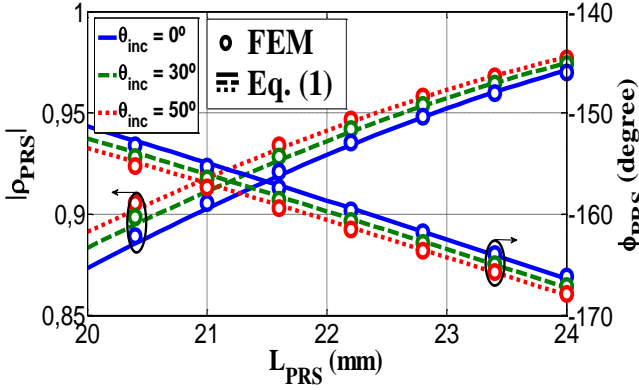


Fig. 3. Reflection coefficient of the PRS (magnitude and phase) seen by a plane wave for different incidence angles as a function of L_{PRS} at 5.6 GHz .

modeling of the tunable HIS. In this case, the following pole-zero expression is employed for Y_{HIS} , which is now dependent on the varactors' junction capacitance C_j :

$$Y_{HIS}(k_y, C_j) = j \frac{[c_j - c_{j_{zn}}(k_y)] \dots [c_j - c_{j_{zn}}(k_y)]}{[c_j - c_{j_{p1}}(k_y)] \dots [c_j - c_{j_{p1}}(k_y)]} \quad (2)$$

In the antenna design, we use a one dimensional version of the tunable HIS configuration proposed in [29,32], so that a row of metallic patches of width $Q_{HIS} = 14\text{ mm}$, length $L_{HIS} = 17\text{ mm}$, separated at a distance $P_{HIS} = 30\text{ mm}$, are printed on Rogers RO 4230 substrate ($\epsilon_{rHIS} = 3$, $D_{HIS} = 1.524\text{ mm}$). Each HIS patch is divided in the x -direction by two equal patches separated by a gap ($g = 1\text{ mm}$) where two varactor diodes are placed as illustrated in Fig.1-b.

As was demonstrated in [25], the boundary condition presented by the changes drastically as the physical resonating length L_{HIS} is varied, thus resulting in a direct mechanism to control the TE_{01} leaky-mode cut-off frequency and therefore the pointing angle at a fixed frequency. Yet, this control could only be mechanically achieved in [25], as the whole PCB should be replaced in order to vary L_{HIS} . The proposed reconfigurable LWA overcomes this disadvantage, since the effective resonant length of the HIS patches can be varied by properly modifying the varactors' junction capacitance C_j [29]. This is shown in Fig.4-a, where the reflection phase presented by the tunable HIS (ρ_{HIS} in Fig.2-b) provides PMC condition ($\phi_{HIS} = 0^\circ$) at different frequencies (5.15 GHz , 5.65 GHz and 6.15 GHz) as C_j is varied (0.35 pF , 0.23 pF , and 0.15 pF). These results were obtained using the pole-zero analytical expression of Y_{HIS} as a function of frequency, for different values of θ_{inc} and C_j . When the frequency is fixed to 5.6 GHz , the behavior of $Y_{HIS}(k_y, C_j)$ can be analytically modeled using (2), obtaining the HIS reflection phase as a function of C_j for different θ_{inc} shown in Fig.4-b. Very good agreement with FEM results is observed for all the range of C_j (from 0 pF to 0.35 pF) and for all incidence angles. The HIS behaves as a transparent sheet for $C_j = 0\text{ pF}$ ($\phi_{HIS} = 150^\circ$), changing to PMC sheet ($\phi_{HIS} = 0^\circ$) for $C_j \approx 0.23\text{ pF}$, and to PEC sheet ($\phi_{HIS} = 180^\circ$) for $C_j = 0.35\text{ pF}$. According to the results reported in [25], increasing C_j corresponds to a larger L_{HIS} , thus showing a direct relation between C_j and the effective resonant length of the HIS patches. Since C_j can be controlled

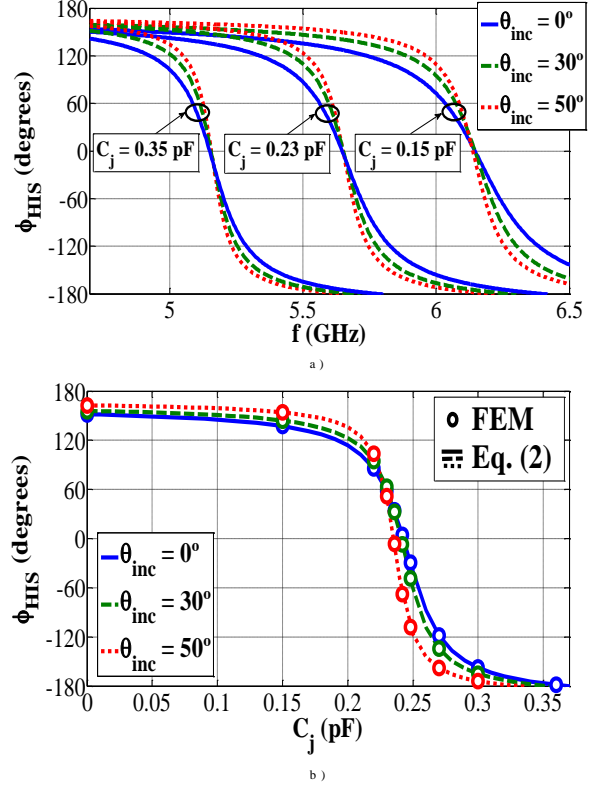


Fig. 4. Reflection phase of the tunable HIS seen by an incident plane wave for different incidence angles a) as a function of frequency for different values of C_j , b) as a function of C_j at 5.6 GHz .

by the varactors' reverse polarization voltage [27]-[34], electronic control of the pointing angle at a fixed design frequency should be possible by combining the 1D FP leaky cavity and the tunable HIS. To theoretically confirm this fact, the behavior of the radiating leaky mode must be studied as a function of C_j .

A. Effect of C_j in the leaky-mode dispersion curves.

Obtaining the leaky-mode dispersion curves as a function of C_j is essential for the electronic beam steering application presented. The unknown leaky-mode complex wavenumber $k_y = \beta_y - j\alpha_y$ can be obtained from the TEN shown in Fig.2, by solving the corresponding Transverse Resonance Equation (TRE) [25],[37]:

$$Y_{UP}(f, k_y, L_{PRS}) + Y_{DOWN}(f, k_y, C_j) = 0 \quad (3)$$

Fig.5 shows the frequency dispersion for the normalized phase (β_y/k_0) and leakage (α_y/k_0) constants as C_j is varied from 0.1 pF to 0.23 pF . As expected, the TE_{01} leaky-mode cutoff frequency decreases as C_j increases. This results in a continuous rise of the leaky-mode phase constant at a fixed frequency as C_j is increased, as it is shown in Fig.5-c for 5.6 GHz . Again, very good agreement is obtained between TRM and full-wave FEM results, validating the proposed TEN. As it can be seen in Fig.5-c, β_y/k_0 is varied from values close to zero when $C_j = 0.1\text{ pF}$, to values close to one when $C_j = 0.23\text{ pF}$. Since the leaky-mode pointing angle is given by $\sin \theta_{RAD} \approx \beta_y/k_0$, it is expected that fixed-frequency beam-scanning from broadside to endfire can be realised by controlling C_j in the aforementioned range [0.1 pF , 0.23 pF].

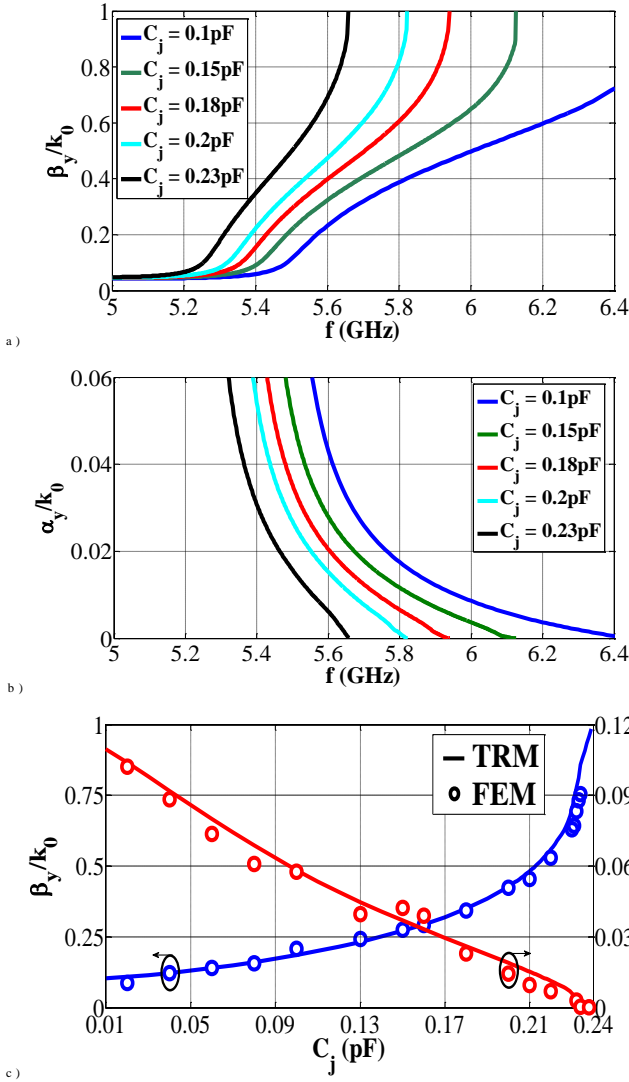


Fig. 5. Leaky-mode dispersion curves as a function of C_j ($L_{PRS}=22\text{ mm}$) a-b) Dispersion with frequency c) Dispersion with C_j at 5.6 GHz .

To give more physical insight into the working principle of the proposed reconfigurable LWA, Fig.6 illustrates the TE_{01} leaky-mode electric field distribution in the cross section of the FP cavity for different values of C_j at the design frequency of 5.6 GHz . For low values of C_j the HIS behaves as a transparent sheet as shown in Fig.4-b and the leaky-mode is resonating in the metallic cavity of height H , providing maximum horizontal field at $z=H/2$, as it can be seen in Fig.6 for $C_j=0.01\text{ pF}$. However, as C_j is increased to 0.23 pF , the HIS tends to behave as a PMC sheet which induces maximum field at its interface, as shown in Fig.6. The boundary conditions seen by the leaky-mode resonating in the FP cavity are strongly changed as C_j is varied. As a result, the leaky-mode transverse wavelength λ_z is modified from $\lambda_z=2H$ when $C_j=0.01\text{ pF}$ to $\lambda_z=4H$ when $C_j=0.23\text{ pF}$, as illustrated in Fig.6. This enlargement in the transverse wavelength λ_z implies the subsequent reduction in the longitudinal wavelength λ_y , and therefore a rise in the leaky-mode longitudinal phase constant ($\beta_y=2\pi/\lambda_y$) as C_j is increased, as predicted by the results shown in Fig.5-c.

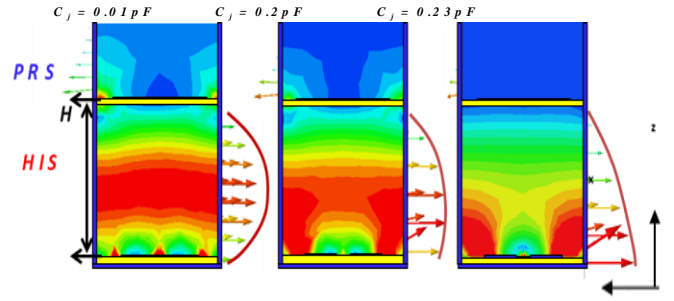


Fig. 6. Leaky-mode electric-field pattern inside the FP PRS-tunable HIS cavity (obtained from FEM) at 5.6 GHz for different values of C_j .

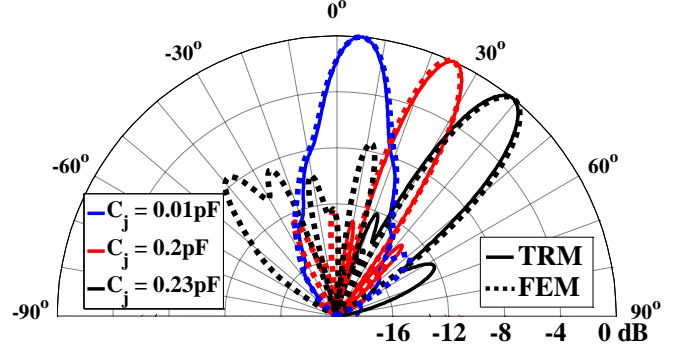


Fig. 7. Computed H-plane normalized radiation patterns for the proposed reconfigurable LWA at 5.6 GHz for different C_j (antenna length $L_A=5\lambda_0$)

Once the leaky-mode complex propagation constant has been obtained as a function of C_j , the associated H-plane radiation pattern can be directly obtained [2], as shown in Fig.7 for the case of a LWA of length $L_A=5\lambda_0$ at 5.6 GHz . As expected, the scanning angle θ_{RAD} is swept from nearly broadside towards the endfire direction as C_j is increased, following the β_y/k_0 curve plotted in Fig.5-c. Particularly, Fig.7 shows the results for $C_j=0.01\text{ pF}$ ($\beta_y/k_0\approx 0.09$, $\theta_{RAD}\approx 5^\circ$), $C_j=0.2\text{ pF}$ ($\beta_y/k_0\approx 0.42$, $\theta_{RAD}\approx 25^\circ$), and $C_j=0.23\text{ pF}$ ($\beta_y/k_0\approx 0.65$, $\theta_{RAD}\approx 40^\circ$). The beam direction and the beam width predicted from the TRM are in very good agreement with full-wave FEM simulations performed in a 3D model of the whole reconfigurable LWA. A strong reflected lobe appears for $C_j=0.23\text{ pF}$, due to the very low leakage-rate associated with high values of C_j (see Fig.5-c), which results in poor radiation efficiency and a large amount of energy being reflected at the far-end of the LWA. This fact limits the maximum scanning angle of the proposed reconfigurable LWA to 40° , as it will be explained in detail in Section III.

B. Optimization of the Fabry-Perot cavity height H .

The physical height of the FP cavity (H) is a key geometrical parameter which determines the scanning range of the proposed reconfigurable LWA. All previous results were computed using the optimum value $H=H_{opt}=25.2\text{ mm}$. As can be seen in Fig.8, a wider scanning range is obtained in this case, so that the cavity height makes the leaky-mode cut-off condition ($\theta_{RAD}\approx 0^\circ$) to be coincident with the minimum value of C_j . In this situation, the dynamic range of the varactors is fully used and the minimum scanning angle is close to broadside. On the other hand, as discussed in [39], the maximum achievable pointing angle in this type of 1D LWA

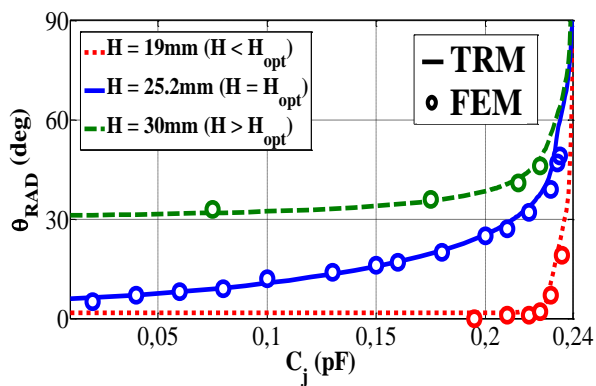


Fig. 8. Leaky-mode scanning-angle as a function of C_j for different values of the Fabry-Perot cavity height, H , at 5.6 GHz .

is produced when the HIS presents a PMC resonance (which in our case corresponds to the value $C_j = 0.23\text{ pF}$).

Above the HIS PMC resonance, a sudden fall of the leakage rate and a rapid divergence of the phase constant as shown in Fig.5-c limit the scanning range to higher angles. Fig.8 shows that for $H = H_{opt}$ the scanning angle can be swept from $\theta_{RAD} = 5^\circ$ for $C_j = 0.01\text{ pF}$ to $\theta_{RAD} = 40^\circ$ for $C_j = 0.23\text{ pF}$, as previously described. However, if $H > H_{opt}$, the minimum value of $C_j = 0$ does not correspond to the leaky-mode cut-off point ($\theta_{RAD} \approx 0^\circ$) but to a higher scanning state. As a result, the minimum scanning angle is located further from broadside ($\theta_{RAD} = 30^\circ$ at $C_j = 0.01\text{ pF}$ in Fig.8 for $H = 30\text{ mm}$). Since the maximum pointing angle given by the HIS PMC resonance ($C_j = 0.23\text{ pF}$) is $\theta_{RAD} = 40^\circ$, the scanning range is reduced to $[30^\circ, 40^\circ]$ instead of $[5^\circ, 40^\circ]$. On the other hand, for shorter FP cavities ($H < H_{opt}$, shown in dotted red line in Fig.8) the leaky mode is below cutoff for most of the range of variation of C_j . As it can be seen in Fig.8 for $H = 19\text{ mm}$, the leaky mode is below cutoff from $C_j = 0\text{ pF}$ to $C_j = 0.2\text{ pF}$, missing this region of the varactors' dynamic range. As a result, the scanning starts at $C_j = 0.2\text{ pF}$ with $\theta_{RAD} = 0^\circ$, but then it is very soon limited to a maximum angle of $\theta_{RAD} = 20^\circ$ at $C_j = 0.23\text{ pF}$. The scanning range has now been reduced to $[0^\circ, 20^\circ]$ instead of $[5^\circ, 40^\circ]$. Figure 8 also shows that the optimum cavity provides the most linear dependence between θ_{RAD} and C_j . Once more, excellent agreement is found in the validation of the TRM dispersion curves and FEM results. In the next sections, the beam scanning mechanism that has been theoretically predicted is demonstrated by experimental results.

III. EXPERIMENTAL RESULTS

The following section describes the experimental results carried out on a prototype fabricated at *CSIRO ICT Centre*, shown in Fig.9. The antenna is designed to operate at the fixed frequency of 5.6 GHz , and the radiating aperture has a length of $L_A = 5\lambda_0$. As illustrated in Fig.9-a, three constituent parts in the reconfigurable LWA can easily be distinguished: a parallel-plate waveguide, a passive PRS printed-circuit, and a tunable HIS. To excite the TE_{01} leaky-mode of the tunable 1D FP cavity, a horizontal coaxial probe is used as proposed in [25]. The dimensions of this feeding probe were optimized to obtain maximum input matching at the operating midpoint of

$C_j = 0.15\text{ pF}$ in order to obtain good matching across most of the dynamic range of C_j .

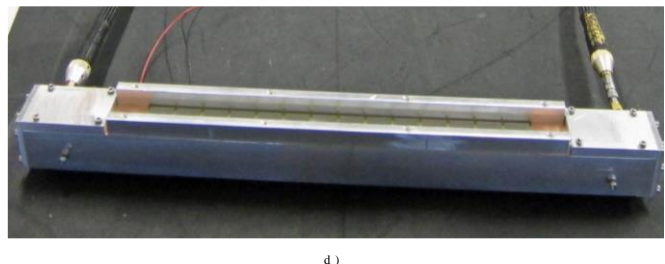
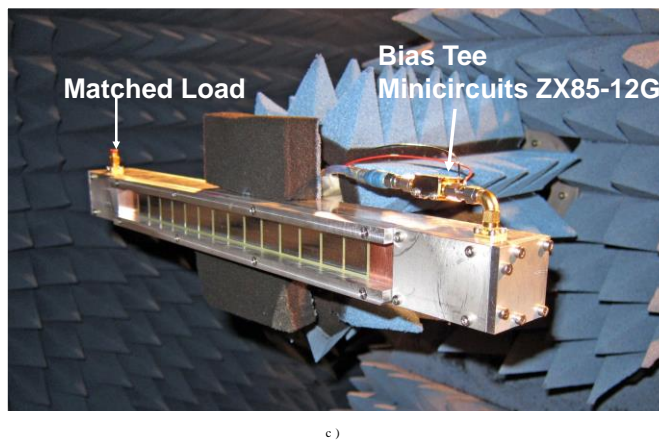
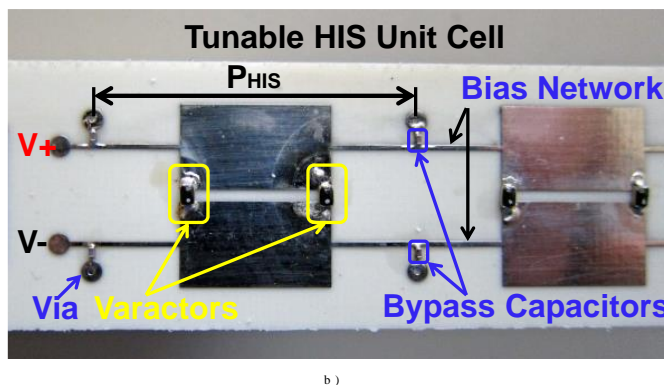
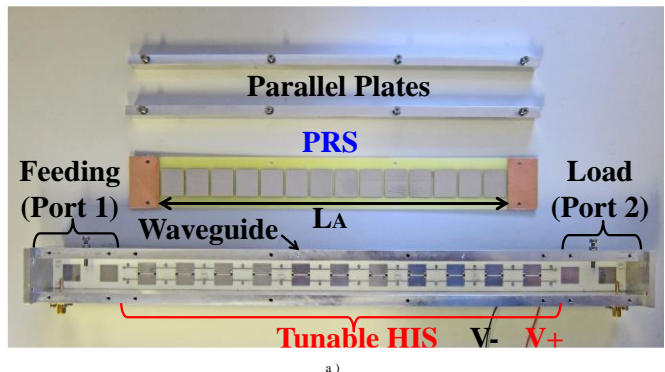


Fig. 9. Photographs of a) Manufactured reconfigurable LWA prototype b) tunable HIS phase agile cell c) Radiation pattern measurement experimental set-up and d) S parameters measurements set-up.

A detailed photograph of the phase agile cell used for the tunable HIS, including the biasing network proposed in [32], is depicted in Fig.9-b. Metelics' MGV125-08 varactor diodes (0805 package) are used for the tunable HIS, providing a range in C_j from 0.055 pF to 0.6 pF as reverse bias voltage V_{ris}

tuned from $20V_{DC}$ to $2V_{DC}$. The varactor's tolerance for C_j is $\pm 0.05pF$ according to the manufacturer datasheet.

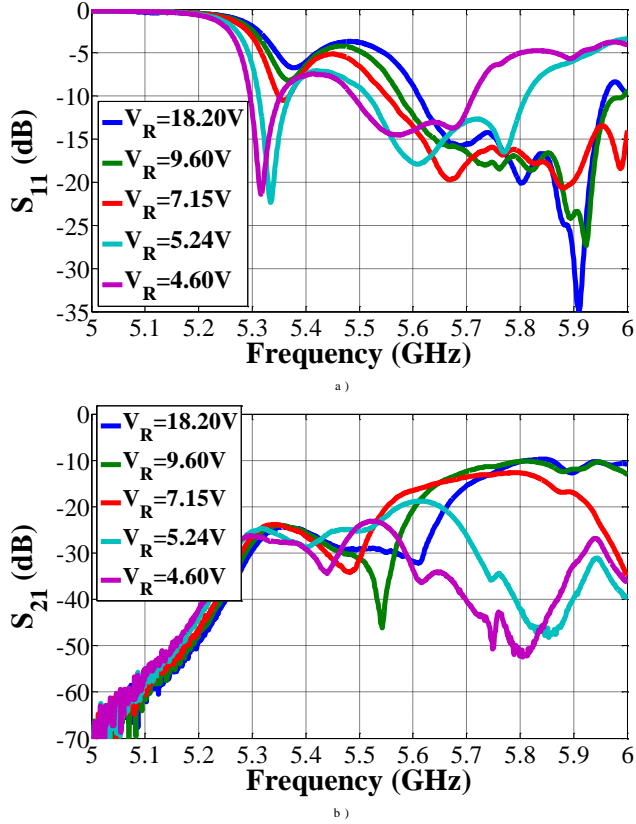


Fig. 10. Measured S parameters vs frequency for different V_R . a) S_{11} , b) S_{21} .

The measured S parameters in the $5GHz-6GHz$ frequency range are presented in Fig.10 for different values of bias voltage V_R . As expected, the matching band is shifted to lower frequencies as V_R is decreased (and C_j is increased), in accordance with the expected theoretical shift in the leaky-mode frequency dispersion presented in Fig.5. These results are also consistent with data reported in previous reconfigurable LWAs using varactors[27-34]. At the fixed operation frequency of $5.6GHz$, Fig.11 shows the simulated and measured S parameters as a function of V_R . As expected, the matching (S_{11}) and the transmission (S_{21}) coefficients are affected as V_R (C_j) is varied. Simulated data predict optimum operation with $S_{11} = -23.7dB$ and $S_{21} = -9.54dB$ for $V_R = 7.17V_{DC}$ (which corresponds to $C_j = 0.15pF$, according to the datasheet).

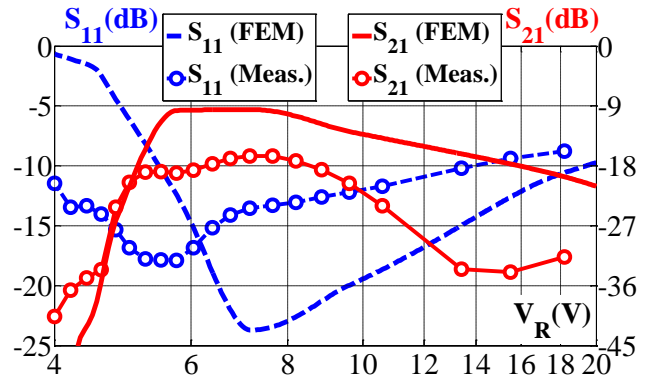


Fig. 11. Measured S parameters vs V_R at $5.6GHz$.

As V_R is varied from this value of $7.17V_{DC}$, the TE_{01} leaky-mode field distribution is strongly perturbed (as it was theoretically illustrated in Fig.6), thus decreasing the matching between the coaxial probe and the FP cavity. It is important to note that, as previously mentioned, the coaxial probe dimensions were optimized for the aforementioned operating point $C_j = 0.15pF$ ($V_R = 7.17V_{DC}$). As a result, poorer matching is obtained at other operation points of the varactor's dynamic range. In particular, the mismatch increases up to $S_{11} = -2dB$ for $V_R = 4.5V_{DC}$ ($C_j = 0.24pF$) and to $S_{11} = -10.6dB$ for $V_R = 18.2V_{DC}$ ($C_j = 0.06pF$). Experimental data report a similar tendency for the measured S parameters as a function of V_R , obtaining $S_{11} = -17.9dB$ and $S_{21} = -19dB$ at the optimum tuning point $V_R = 5.75V$ ($C_j = 0.19$) and similar deterioration for other values of V_R . As can be seen, measured data is shifted to lower V_R values with respect to simulations. This shift is attributed to the varactors' tolerance errors, as demonstrated next.

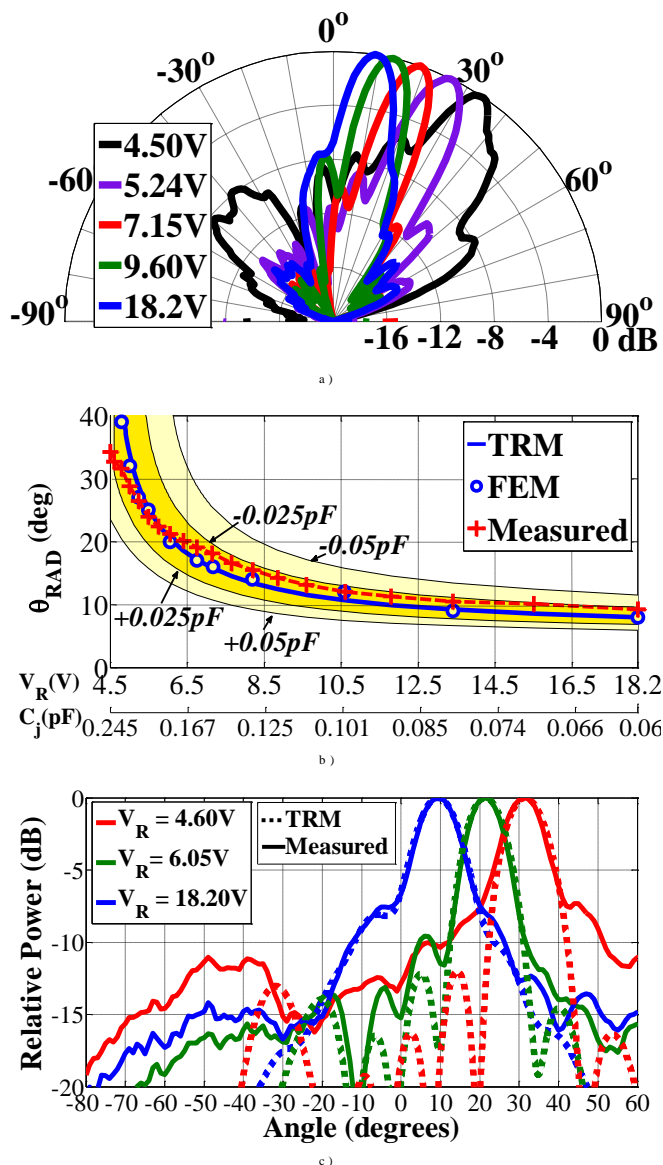


Fig. 12. Radiation response of reconfigurable LWA at 5.6 GHz vs V_R . a) Measured radiation patterns b) Pointing angle scanning c) Comparison between measured and theoretical radiation patterns.

The electronic control over the LWA radiation pattern is shown in Fig.12. Fig.12-a depicts the measured normalized radiation pattern at 5.6 GHz for different values of the applied bias voltage V_R . As it can be seen, the main beam is scanned from $\theta_{RAD} = 9.2^\circ$ for $V_R = 18.2 V_{DC}$ ($C_j = 0.06 pF$) to $\theta_{RAD} = 34.2^\circ$ for $V_R = 4.5 V_{DC}$ ($C_j = 0.245 pF$). Figs.12-b and 12-c show the agreement between theory and experiments. In particular, Fig.12-b plots with red crosses the measured scanning response (θ_{RAD} vs V_R) of the proposed reconfigurable LWA, confirming the continuous electronic scanning from 34.2° to 9.2° as V_R is increased from $4.5 V_{DC}$ to $18.2 V_{DC}$. The theoretical leaky-mode scanning response extracted from the TRM is plotted with a continuous blue line, while FEM simulations are represented with blue circles. Very good agreement is observed between these three set of results. However, the measured scanning response is slightly shifted with respect to TRM and FEM results, showing discrepancies in θ_{RAD} that are below $\pm 2^\circ$. This can be attributed to the aforementioned

$\pm 0.05 pF$ varactors' tolerances in C_j . To demonstrate this fact, error curves computed by applying a shift in C_j of $\pm 0.025 pF$ and $\pm 0.05 pF$ are represented with shaded zones in Fig.12-b. As can be seen, the measured scanning response lies inside the $\pm 0.025 pF$ region, well below the diodes' tolerance ($\pm 0.05 pF$).

Finally, Fig.12-c compares the theoretical leaky-mode and measured radiation patterns for three illustrative values of V_R covering the entire scanning range. Not only the main beam direction is accurately coincident between theory and experiments for all V_R , but also the 3dB beam width and the secondary lobes level and position are well predicted, thus confirming the leaky-mode radiation mechanism for the reconfigurable antenna. To obtain the results of Fig.12-c, the measured pointing angle θ_{RAD} and the requested experimental tuning voltage V_R and associated C_j (according to the nominal V_R - C_j response of the varactors' datasheet) have been used as references for each case. In order to show the discrepancies between the experimental and the theoretical electronic scanning, Table I summarizes the pointing angle θ_{RAD} obtained for three operation points inside the scanning region. As it is shown, maximum error is obtained at lower voltages that correspond to larger scan angles ($V_R = 5 V_{DC}$, $\Sigma \theta_{RAD} = -5.3^\circ$).

TABLE I
BIAS VOLTAGE AND POINTING ANGLE FOR THREE OPERATING POINTS OF THE RECONFIGURABLE LWA

Case	Theory (TRM)	Experiments	Error
$V_R (V_{DC})$	θ_{RAD}	θ_{RAD}	$\Sigma \theta_{RAD}$
5.0	34.1°	28.8°	-5.3°
6.0	20.5°	21.2°	$+0.7^\circ$
20.0	8°	9.2°	$+1.2^\circ$

Finally, Fig.13 summarizes the experimental performance of the reconfigurable LWA in terms of gain and efficiency. Fig.13-a shows the variation of the gain as a function of V_R . Maximum measured gain of $G = 12.95 dBi$ has been obtained for $V_R = 10.6 V_{DC}$ ($C_j = 0.1 pF$, $\theta_{RAD} = 12^\circ$), while simulations predict maximum $G = 12.6 dB$ for $V_R = 9.6 V_{DC}$ ($C_j = 0.11 pF$, $\theta_{RAD} = 11^\circ$).

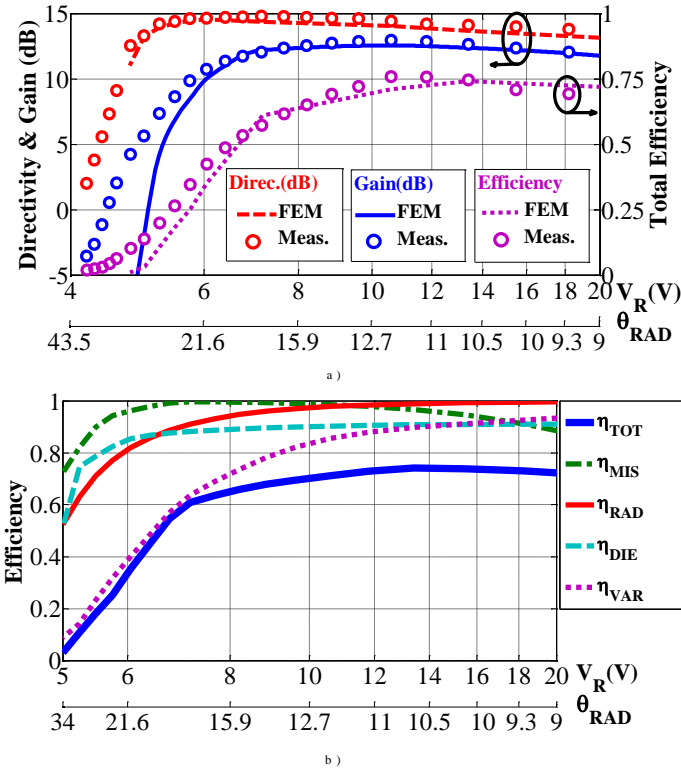


Fig.13. Results at 5.6 GHz vs V_R a) Measured gain, directivity and total efficiency and b) Estimated efficiency and subefficiencies from Full-Wave simulations.

Moreover, as V_R is decreased from this optimum point, a significant drop in the gain is observed. The minimum value of gain measured is $G = -3.55 \text{ dB}$ for $V_R = 4.2 \text{ VDC}$ ($C_j = 0.26 \text{ pF}$), which corresponds to an angle close to $\theta_{RAD} = 35^\circ$. Similar behavior is obtained with simulations, thus making it difficult to obtain large scan angles. As it was previously explained, this fact is caused by higher mismatch (see Fig.11) and by the fall of the leakage rate (see Fig.5-c) that take place at high values of C_j (lower V_R), due to the associated PMC resonance of the HIS for high θ_{RAD} (see Fig.6). However, the LWA shows a stable gain above $G = 10 \text{ dB}$ for $V_R > 6 \text{ VDC}$, which corresponds to scanning angles below $\theta_{RAD} = 25^\circ$. As also plotted in Fig.13-a, this gain translates into a total efficiency $\eta_{TOT} = G/D > 50\%$, reaching $\eta_{TOT} = 75\%$ for $V_R = 10-14 \text{ VDC}$ ($\theta_{RAD} = 13^\circ-10^\circ$). Measured and simulated total efficiency (η_{TOT}) in Fig.13-a are in concordance, observing $\eta_{TOT} > 60\%$ in the range $V_R = 8-20 \text{ VDC}$ ($\theta_{RAD} = 16^\circ-10^\circ$), whereas η_{TOT} tends to 3% for $V_R = 5 \text{ VDC}$ ($\theta_{RAD} > 30^\circ$). To understand the gain and efficiency response of the LWA, Fig.13-b separates η_{TOT} into its different constitutive efficiencies [41,42]:

$$\eta_{TOT} = \eta_{MIS} \cdot \eta_{RAD} \cdot \eta_{DIE} \cdot \eta_{VAR} \quad (4)$$

where the mismatch efficiency is computed from the measured input reflections ($\eta_{MIS} = 1 - |S_{11}|^2$) [41], the leaky-mode radiation efficiency is estimated from the theoretical leakage rate ($\eta_{RAD} = 1 - e^{-2\alpha y L_A}$) [42], and the ohmic efficiency has been attributed to two contributions: one part due to the dielectric losses and another term due to dissipation in the varactors series resistance: $\eta_{\Omega} = \eta_{DIE} \cdot \eta_{VAR}$ [41]. Since the separated ohmic efficiencies (due to dielectrics and varactors)

are difficult to compute from experiments [41], they have been estimated from full-wave simulation data. Equation (4) gives, as a first order approximation, a good insight into the origin of the gain drop for large scan angles. Particularly, it can be seen in Fig.13-b that the mismatch efficiency η_{MIS} is quite high (over 85%) for the entire dynamic range. On the other hand, the leaky-mode radiation efficiency η_{RAD} strongly decreases from 100% at $V_R = 20 \text{ VDC}$ ($\theta_{RAD} = 9^\circ$) to 52% at $V_R = 5 \text{ VDC}$ ($\theta_{RAD} = 30^\circ$), being consistent with the drop of the leakage rate predicted in Fig.5-c for high values of C_j (i.e. high values of θ_{RAD}). The dielectric efficiency results predict a fall from $\eta_{DIE} = 90\%$ at $\theta_{RAD} = 9^\circ$ ($V_R = 20 \text{ VDC}$) to $\eta_{DIE} = 50\%$ at $\theta_{RAD} = 30^\circ$ ($V_R = 5 \text{ VDC}$), which is caused by the electric field concentration at the HIS substrate for the PMC regime (see Fig.6 for $C_j = 0.23 \text{ pF}$). Due to the same high concentration of the modal fields, an increase in the current density flowing across the diodes occurs at this PMC operational point, raising the heat dissipation at their series resistance. As a result, the varactors' ohmic efficiency η_{VAR} strongly drops for scanning angles tending to endfire, observing a decrease from $\eta_{VAR} = 94\%$ at $\theta_{RAD} = 9^\circ$ ($V_R = 18 \text{ VDC}$) to $\eta_{VAR} = 9\%$ at $\theta_{RAD} = 30^\circ$ ($V_R = 5 \text{ VDC}$). This result agrees with other published works that report significant increase in the HIS ohmic losses when operating close to the PMC resonance, and which has even been widely applied to create planar microwave absorbers [44-46]. Therefore, it can be concluded that the gain drop for large scan angles is unavoidable and it is due to two main reasons: the decrease in the leaky-mode radiation efficiency, and the increase in the varactors resistance losses.

IV. CONCLUSIONS

A new type of electronically scannable one-dimensional LWA, which is based on a tunable Fabry-Perot (FP) cavity formed by a Parallel-Plate Waveguide (PPW), a Partially Reflective Surface (PRS), and a varactor-loaded active High Impedance Surface (HIS), has been presented in the paper. The proposed reconfigurable LWA topology allows to electronically modify the resonant condition of the TE_{01} leaky mode inside the FP cavity, resulting in a variation of the pointing direction at a fixed frequency as the varactor bias is changed. Leaky-mode dispersion curves have been obtained from a simple but accurate Transverse Equivalent Network, which rigorously takes into account the effect of the varactors' junction capacitance in the phase response of the active HIS. These modal curves are very useful for the design of the main parameters of the antenna, in order to optimize the beam-scanning range. Leaky-mode results are in very good agreement with full-wave simulations and experiments, which have shown a continuous scanning from 9° to 30° in a prototype operating at the fixed frequency of 5.6 GHz, as the varactors' bias voltage is varied from 20 VDC to 5 VDC . The scanning range is limited in the endfire region due to the drop in the leakage rate and the increase of thermal losses, which are associated with the Perfect Magnetic Conductor (PMC) condition of the tunable High Impedance Surface. An interesting advantage of this new reconfigurable topology resides in its potential application to two-dimensional FP LWAs [32],[33],[35],[40] and to new metasurface LWAs [47],[48], so that the electronic scanning could be extended for

both elevation and azimuthal planes. This type of electronically steerable LWA presents a low-cost potential alternative to more expensive phased-arrays [48].

ACKNOWLEDGMENT

The authors would like to thank Mr Carl Holmesby for fabricating the waveguide, Mr Rob Shaw for soldering the surface mount components, and Mrs. María García-Vigueras for her insightful and interesting comments.

REFERENCES

- [1] R. Fralich and J. Litva, "Beam-steerable active array antenna," *Electron. Lett.*, vol. 28, pp. 184–185, Jan. 1992.
- [2] A.A. Oliner, "Leaky-wave antennas", in *Antenna Engineering Handbook*, 3rd ed, R.C. Johnson, Ed. New York, McGraw-Hill, 1993, Ch. 10.
- [3] C.-C.Hu, C.F. Jou, and J.-J. Wu, "Two-dimensional beam-scanning linear active leaky-wave antenna array using coupled VCOs," *IEE Proc. Microw., Antennas and Propag.*, vol.147, no.1, pp. 68–72, Feb. 2000.
- [4] J. T. Bernhard, K. Chang, Ed., "Reconfigurable antennas," in *The Wiley Encyclopedia in The Wiley Encyclopedia of RF and Microwave Engineering*. New York: Wiley, Feb. 2005.
- [5] R. E. Horn, H. Jacobs, E. Freibergs, and K. L. Klohn, "Electronic modulated beam steerable silicon waveguide array antenna," *IEEE Trans. Microwave Theory Tech.*, vol.28, pp. 647–653, June 1980.
- [6] H. Maheri, M. Tsutsumi, and N. Kumagi, "Experimental studies of magnetically scannable leaky-wave antennas having a corrugated ferrite slab/dielectric layer structure," *IEEE Trans. Antennas Propag.*, vol. 36, pp. 911–917, Nov. 1988.
- [7] V.K. Varadan, V.V. Varadan, K.A. Jose, and J.F. Kelly, "Electronically steerable leaky wave antenna using a tunable ferroelectric material," *Smart Mater. Struct.*, vol. 3, pp. 470–475, June 1994.
- [8] V. A. Manasson, L. S. Sadovnik, A. Mousessian, and D. B. Rutledge, "Millimeter-wave diffraction by a photo-induced plasma grating," *IEEE Trans. Microwave Theory Tech.*, vol. 43, pp. 2288–2290, Sept. 1995.
- [9] A. Alphones and M. Tsutsumi, "Leaky wave radiation from a periodically photoexcited semiconductor slab waveguide," *IEEE Trans. Microwave Theory Tech.*, vol. 43, pp. 2435–2441, Sept. 1995.
- [10] L. Huang, J. Chiao, and P. Lisio, "An electronically switchable leaky wave antenna," *IEEE Trans. Antennas Propag.*, vol. 48, pp.1769–1772, Nov. 2000.
- [11] C.-C. Chen and C.-K.C Tzuang, "Phase-shifterless beam-steering microslotline antenna," *Electron. Lett.*, vol.38, no.8, pp. 354–355, April 2002.
- [12] A. Grbic, and G.V. Eleftheriades, "Leaky CPW-based slot antenna arrays for millimeter-wave applications," *IEEE Trans. Antennas Propag.*, vol.50, no.11, pp. 1494–1504, Nov. 2002.
- [13] K.M. Noujeim, "Wave propagation characteristics of a reactively loaded microstrip," *IEEE MTT-S Int. Microwave Symposium Digest*, vol.2, pp. 821–824, June 2003.
- [14] M. Zulfiani, A. Petosa, A. Ittipiboon, L. Roy, and R. Chaharmir, "Microstrip periodic leaky-wave antenna with optical control and beam scanning capabilities," *IEEE Antennas and Propag. Society Int. Symposium*, vol.2, pp. 1831–1834, 20–25 June 2004.
- [15] S. Lim, C. Caloz, and T. Itoh, "Electronically scanned composite right/left handed microstrip leaky-wave antenna," *IEEE Microwave and Wireless Components Lett.*, vol.14, no. 6, pp. 277–279, June 2004.
- [16] S. Lim, C. Caloz, and T. Itoh, "Metamaterial-based electronically controlled transmission-line structure as a novel leaky-wave antenna with tunable radiation angle and beamwidth," *IEEE Trans. Antennas Propag.*, vol.52, no.12, pp. 2678–2690, Dec. 2004.
- [17] Y. Yashchyshyn, and J. Modelski, "Rigorous analysis and investigations of the scan antennas on a ferroelectric substrate," *IEEE Trans. Microwave Theory Tech.*, vol. 53, no. 2, pp. 427–438, Feb. 2005.
- [18] G. Augustin, S.V. Shynu, C.K. Anandan, P. Mohanan, and K. Vasudevan, "A novel electronically scannable log-periodic leaky-wave antenna," *Microw. and Opt. Techn. Lett.*, vol. 45, no. 2, pp. 163–165, April 2005.
- [19] Y. Yashchyshyn, and J. Modelski, "A reconfigurable leaky-wave microstrip antenna," *2005 European Microwave Conference*, vol. 1, pp. 2005.
- [20] Y. Li and Y. Long, "Frequency-fixed beam-scanning microstrip leaky-wave antenna with multi-terminals," *Electron. Lett.*, vol. 42, no. 1, pp. 7–8, Jan. 2006.
- [21] Y. Li, Q. Xue, E.K.-N. Yung, and Y. Long, "Dual-beam steering microstrip leaky wave antenna with fixed operating frequency," *IEEE Trans. Antennas Propag.*, vol.56, no.1, pp. 248–252, Jan. 2008.
- [22] M. Archbold, E.J. Rothwell, L.C. Kempel, and S.W. Schneider, "Beam steering of a half-width microstrip leaky-wave antenna using edge loading," *IEEE Antennas and Wireless Propag. Lett.*, vol. 9, no. 2, pp. 203–206, 2010.
- [23] A. Suntives, and S.V. Hum, "An electronically tunable half-mode substrate integrated waveguide leaky-wave antenna," *Antennas and Propagation (EUCAP), Proceedings of the 5th European Conference on*, pp. 3670–3674, April 2011.
- [24] R. Ouegraogo, E. Rothwell, and B. Greetis, "A reconfigurable microstrip leaky-wave antenna with a broadly steerable beam," *IEEE Trans. Antennas Propag.*, vol.59, no.8, pp. 3080–3083, Aug. 2011.
- [25] M. García-Vigueras, J.L. Gómez-Tornero, G. Goussetis, A. R. Weily, and Y.J. Guo, "1D-leaky wave antenna employing parallel-plate waveguide loaded with PRS and HIS," *IEEE Trans. Antennas Propag.*, vol. 59, no. 10, pp. 3687–3694, Oct. 2011.
- [26] J. L. Gómez, D. Cañete and A. Álvarez-Melcón, "Printed-circuit leaky-wave antenna with pointing and illumination flexibility," *IEEE Microw. Wireless Compon. Lett.*, vol. 15, no. 8, pp. 536–538, Aug. 2005.
- [27] D. Sievenpiper and J. Schaffner, "Beam steering microwave reflector based on electrically tunable impedance surface," *Electron. Lett.*, vol. 38, no. 21, pp. 2111–2112, Oct. 2002.
- [28] D. F. Sievenpiper, J. H. Schaffner, H. J. Song, R. Y. Loo, and G. Tanganan, "Two-Dimensional beam steering using an electrically tunable impedance surface," *IEEE Trans. Antennas Propag.*, vol. 51, pp. 2713–2722, Oct. 2003.
- [29] S. V. Hum, M. Okoniewski, and R. J. Davies, "Realizing an electronically tunable reflectarray using varactor diode-tuned elements," *IEEE Microw. Wireless Compon. Lett.*, vol. 15, no. 6, pp. 422–424, June 2005.
- [30] C. Mias, and J.H. Yap, "A varactor-tunable high impedance surface with a resistive-lumped-element biasing grid," *IEEE Trans. Antennas Propag.*, vol. 55, no. 7, pp. 1955–1962, July 2007.
- [31] D.F. Sievenpiper, "Forward and backward leaky wave radiation with large effective aperture from an electronically tunable textured surface," *IEEE Trans. Antennas Propag.*, vol. 53, no. 1, Jan. 2005.
- [32] A.R. Weily, T.S. Bird, and Y.J. Guo, "A reconfigurable high-gain partially reflecting surface antenna," *IEEE Trans. Antennas Propag.*, vol. 56, no. 11, pp. 3382–3390, Nov. 2008.
- [33] F. Costa and A. Monorchio, "Design of subwavelength tunable and steerable Fabry-Perot / leaky-wave antennas," *Progress In Electromagnetics Research*, vol. 111, pp. 467–481, 2011.
- [34] F. Costa, A. Monorchio, S. Talarico, and F. M. Valeri, "An active high impedance surface for low profile tunable and steerable antennas," *IEEE Antennas and Wireless Propagation Letters*, vol. 7, pp. 676–680, 2008.
- [35] T. Zhao, D.R Jackson, J.T. Williams, H.-Y.D Yang, A.A Oliner, "2-D periodic leaky-wave antennas-part I: metal patch design," *IEEE Trans. Antennas Propag.*, vol. 53, no. 11, pp. 3505–3514, Nov. 2005.
- [36] T. Zhao, D. R. Jackson, J. T.Williams, and A. A. Oliner, "Simple CAD model for a dielectric leaky-wave antenna," *IEEE Antennas Wireless Propag. Lett.*, vol. 3, pp. 243–245, 2004.
- [37] M. García-Vigueras, J.L. Gómez-Tornero, G. Goussetis, J.S. Gómez-Díaz, and A. Álvarez-Melcón, "A modified pole-zero technique for the synthesis of waveguide leaky-wave antennas loaded with dipole-based FSS," *IEEE Trans. Antennas Propag.*, vol. 58, no. 6, pp. 1971–1979, June 2010.
- [38] S. Maci, M. Caiazzo, A. Cucini, and M. Casaletti, "A pole-zero matching method for EBG surfaces composed of a dipole FSS printed on a grounded dielectric slab," *IEEE Trans. Antennas Propag.*, vol. 53, no. 1, pp. 70–81, Jan. 2005.
- [39] M. García-Vigueras, J.L. Gómez-Tornero, G. Goussetis, Andrew R. Wiley, and Y. Jay Guo, "Enhancing frequency-scanning response of leaky-wave antennas using high impedance surfaces," *IEEE Antennas and Wireless Propag. Lett.*, vol. 10, pp. 7–10, March 2011.
- [40] A.P. Feresidis, G. Goussetis, S. Wang and J.C. Vardaxoglou, "Artificial magnetic conductor surfaces and their application to low-profile high-gain planar antennas," *IEEE Trans. Antennas Propag.*, vol. 53, no. 1, pp. 209–215, Jan. 2005.
- [41] C.A. Balanis, *Antenna Theory*, Singapore: John Wiley and Sons, 2nd Ed., 1982, ch.2.8, "Antenna Efficiency", pp.60–61.

- [42] J.L. Gómez, G. Goussetis and A.A. Melcón, "Correction of dielectric losses in leaky-wave antenna designs," *Journal of Electromagnetic Waves and Applications*, vol.21, no. 8, pp.1025-1036,2007.
- [43] D.M. Pozar, *Microwave Engineering*, John Wiley and Sons, 2nd Ed., 1998, ch.3, "Transmission Lines and Waveguides", pp.111.
- [44] S.A. Tretyakov and S I. Maslovski, "Thin absorbing structure for allincidence angles based on the use of a high-impedance surface," *Microw.Opt.Technol.Lett.*, vol.38, no. 3, pp. 175-178, Aug.2003
- [45] N. Engheta, "Thin absorbing screens using metamaterial surfaces," in *Proc. IEEE Antennas Propagation Soc. Int. Symp.*, 2002, vol. 2, pp. 392-395.
- [46] F. Costa, A. Monorchio, G. Manara, "Analysis and design of ultra thin electromagnetic absorbers comprising resistively loaded high impedance surfaces," *IEEE Trans. Antennas Propag.*, vol. 58, no. 5, pp. 1551, 2010.
- [47] G. Minatti, F. Caminita, M. Casaletti, S. Maci, "Spiral leaky-wave antennas based on modulated surface impedance," *IEEE Trans. Antennas Propagat.*, vol. 59, no. 12, pp. 4436 - 4444, Nov. 2011.
- [48] "Intellectual ventures invents beam-steering metamaterials antenna IV and others aim at cheap in-flight broadband," by Katie M. Palmer, *IEEE Spectrum Magazine*, Nov. 2011.